AGU PUBLICATIONS

JGR

Journal of Geophysical Research: Space Physics

RESEARCH ARTICLE
10.1002/2016JA022754

Key Points:
- Measurements of current density around dipolarization fronts
- Observations of current density reduction ahead of dipolarization fronts
- Current density reduction caused by ion reflection and electrostatic field

Correspondence to:
S. Lu,
slu@igpp.ucla.edu

Citation:
Lu, S., A. V. Artemyev, V. Angelopoulos, Q. Lu, and J. Liu (2016), On the current density reduction ahead of dipolarization fronts, *J. Geophys. Res. Space Physics*, *121*, 4269–4278, doi:10.1002/2016JA022754.

Received 28 MAR 2016
Accepted 27 APR 2016
Accepted article online 29 APR 2016
Published online 14 MAY 2016

On the current density reduction ahead of dipolarization fronts

San Lu[1], A. V. Artemyev[1], V. Angelopoulos[1], Quanming Lu[2], and Jiang Liu[1]

[1]Department of Earth, Planetary, and Space Sciences, and Institute of Geophysics and Planetary Physics, University of California, Los Angeles, California, USA, [2]CAS Key Laboratory of Geospace Environment, Department of Geophysics and Planetary Sciences, University of Science and Technology of China, Hefei, China

Abstract During their earthward propagation, dipolarization fronts (DFs) interact with the ambient plasma sheet on kinetic scales. The interaction region is important to the front's structure, propagation, and regional closure of the current system. However, the physics in this region, especially of its current system, is poorly understood. We present Time History of Events and Macroscale Interactions during Substorms (THEMIS) observations of the interaction region between DFs and the ambient plasma sheet at $x \sim -12\,R_E$ downtail; these observations show that the current density ahead of the DFs is significantly reduced near the neutral plane. We use a two-dimensional particle-in-cell model to simulate the current density reduction ahead of DFs and investigate the physical mechanism that causes it: Ion reflection and acceleration at the front cause positive charge density to build up. The resultant electrostatic field, E_z, is directed away from the neutral plane. The positive cross-tail $E_z \times B_x$ drift of electrons (which remain magnetized) does not affect demagnetized ions. This electron-ion decoupling results in a dawnward cross-field current carried by electrons that reduces the cross-tail current ahead of the approaching front.

1. Introduction

Dipolarization fronts (DFs), transient increases in the northward magnetic field component, B_z, in the Earth's magnetotail plasma sheet, have been observed by spacecraft for decades [*Russell and McPherron*, 1973; *Moore et al*., 1981; *Angelopoulos et al*., 1992; *Nakamura et al*., 2002; *Runov et al*., 2009, 2011a, 2011b; *Schmid et al*., 2011, 2015; *Fu et al*., 2012a, 2012b]. Often preceded by a smaller B_z decrease [e.g., *Nakamura et al*., 2002; *Sitnov et al*., 2009; *Lu et al*., 2015], DFs are embedded within bursty bulk flows [*Angelopoulos et al*., 1992, 1994], which are widely believed to play a crucial role in earthward transport of energy and flux [*Angelopoulos et al*., 1992, 2013; *Nakamura et al*., 2011; *Liu et al*., 2011, 2014; *Li et al*., 2016]. Dipolarization fronts energize and inject particles [*Fu et al*., 2011, 2013; *Gabrielse et al*., 2012, 2014; *Ganushkina et al*., 2013; *Lin et al*., 2014] and drive a variety of waves [*Sergeev et al*., 2009; *Deng et al*., 2010; *Huang et al*., 2012; *Panov et al*., 2013]. Reflected and accelerated by approaching DFs [*Zhou et al*., 2010; *Wu and Shay*, 2012; *Eastwood et al*., 2015], ions from the ambient plasma sheet compose earthward precursor flows to the front [*Zhou et al*., 2011]. These ions also create a local density/pressure enhancement that works against the curvature force, moderating the DFs' initial acceleration and contributing to its eventual stoppage [*Li et al*., 2011; *Zhou et al*., 2014a].

Recently, multispacecraft observations have been used to study the current system of DFs. Time History of Events and Macroscale Interactions during Substorms (THEMIS) observations have revealed a strong duskward current density within DFs (about 10 times larger than the cross-tail current density ahead of them) [*Runov et al*., 2011b; *Liu et al*., 2013a]. Cluster observations have demonstrated that when DFs are preceded by transient B_z decreases, the current within those decreases is often dawnward [*Yao et al*., 2013]. According to THEMIS and Cluster observations, DFs also carry field-aligned currents that form a current "wedgelet" [*Liu et al*., 2013a, 2013b; *Sun et al*., 2013], and *Liu et al*. [2015] suggested that several wedgelets combined compose a large-scale substorm current wedge [*McPherron et al*., 1973]. Thus, the current closure around DFs can have implications for the global magnetospheric current system.

Although reflected ions act on the DF's current system and the cross-tail current sheet, how these systems interact in the region between them is poorly understood. Test particle modeling with a prescribed electromagnetic field for the cross-tail current sheet and the approaching front has shown, to first order, that observations are consistent with a simple picture of ion reflection without feedback to the fields [*Zhou et al*., 2011, 2014b; *Ukhorskiy et al*., 2013; *Greco et al*., 2014]. In principle, however, reflected ions

observed near DFs could modify the configuration of the cross-tail current sheet ahead of fronts. Recent observations of that current sheet near the neutral plane have revealed a significant duskward current density reduction associated with pressure buildup near the front [*Yao et al*., 2015]. Similar reduction was derived from multifluid model [*Yang et al*., 2012]. The dawnward current that leads to this reduction may be generated by reflected ion currents [*Zhou et al*., 2014b; *Pan et al*., 2015] or pressure gradient buildup [*Yao et al*., 2015]. These mechanisms, which arise from evolution of ions in prescribed fields, have not been verified by self-consistent kinetic models of DF propagation in the presence of ion-electron interactions in this kinetic regime.

It is important to understand this current density reduction because it affects the interaction of the DF with the medium it encounters just upstream of it and the redistribution (local or global) of the DF's current system during its propagation. The interaction of the magnetic field fronts (with plasma flows) with their surrounding current sheets is rather common because of the transience of magnetic reconnection in planetary magnetospheres and the solar corona. An investigation of the structure of the interface between the magnetotail current sheet and DFs can improve our understanding of this interesting intermediate region where magnetic energy is converted to energy of reflected ions and where electromagnetic waves are generated. In this paper, we present THEMIS observations of current density reduction ahead of dipolarization fronts and use two-dimensional (2-D) particle-in-cell (PIC) model to simulate this reduction and determine how it occurs.

2. THEMIS Observations

We examine THEMIS observations from October to December 2015, when the three THEMIS spacecraft (ThA, ThD, and ThE) traversed the nightside magnetotail near $x \sim -12\ R_E$ (GSM coordinates are used throughout this paper). There are two main advantages of this data set.

1. During this time the three THEMIS spacecraft often formed a triangle with separation of approximately 1000–5000 km, predominantly lying in the (x, z) plane and near the magnetic equator. The small y separation between the spacecraft allows us to obtain accurate derivatives in the x and z directions, ignoring the typically smaller variation of plasma sheet quantities along y. Thus, we can regularly apply the curlometer technique [*Dunlop et al*., 2002] for THEMIS measurements of the magnetic field in two dimensions and obtain the average duskward directed current density in the region between the spacecraft.
2. The magnetic field gradients (in the background current sheet and at the DF) are much stronger in the near-Earth region ($x \sim -12\ R_E$), where THEMIS spacecraft are located, than in the midtail ($x \sim -18\ R_E$) region, where the Cluster mission previously collected most of its DF observations [e.g., *Schmid et al*., 2011; *Fu et al*., 2012b]. Thus, the THEMIS spacecraft can measure both the strong current density at DFs and the much weaker (but still significant) cross-tail current density in the background current sheet, allowing us to unambiguously detect current density reduction (relative to the unperturbed current sheet) ahead of the DF.

We use magnetic field measurements with 3 s (spin period) resolution [*Auster et al*., 2008] and combined moments of electrons and ions from the THEMIS electrostatic analyzer [*McFadden et al*., 2008] and solid state telescope [e.g., *Angelopoulos et al*., 2008]. The curlometer technique [*Dunlop et al*., 2002] is used, except with 2-D (gradients only in the (x, z) plane), and we calculate both $\partial B_x/\partial z$ and $\partial B_z/\partial x$ (the main current density component is $j_y = (\partial B_x/\partial z - \partial B_z/\partial x)/\mu_0$).

Three THEMIS spacecraft observed a DF near the neutral plane (see Figure 1). At least one spacecraft measured $|B_x| < 10$ nT (not shown here), indicating that the triad were near the magnetic equator. As shown in Figure 1a, all three THEMIS spacecraft observed a B_z increase (from 10 to 20 nT). As expected, the most tailward ThA detected an increasing B_z first, signifying DF arrival from the tail. The B_z increase was subsequently observed by ThD and ThE. This DF's earthward velocity was about 100 km/s (low for this region [see *Liu et al*., 2014]). The sharpest B_z increase was observed by ThE, which was located in the neutral plane ($B_x \approx 0$); ThA ($B_x \approx 15$ nT) and ThD ($B_x \approx -10$ nT) observed smoother DF profiles. Near the beginning of the plotted interval, the current density in the background current sheet was about $j_y \approx 5$ nA/m^2. Just ahead of the DF, j_y dropped to zero; at the DF itself, j_y reached 25 nA/m^2. The plasma temperature (ion and electron) increased and the density decreased in the DF region relative to those in the pre-DF region (a typical evolution near a DF [see, e.g., *Runov et al*., 2015; *Schmid et al*., 2015, and references therein]). The plasma velocity V_x shown for ThE (closer to the neutral plane) started growing from zero ahead of the DF and reached its maximum value,

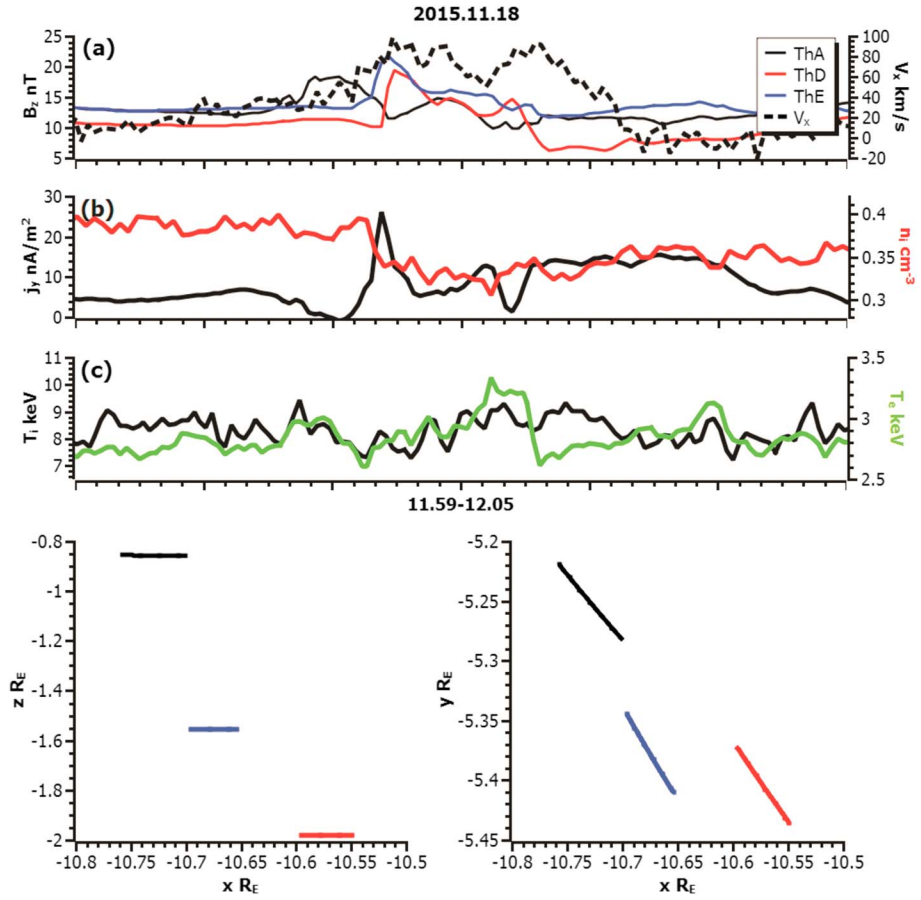

Figure 1. A DF observed by three THEMIS spacecraft. (a) Three profiles of the B_z magnetic field (left vertical axis) and ion bulk velocity V_x measured near the neutral plane (right vertical axis). (b) Profiles of current density (black, left vertical axis) and plasma density measured near the neutral plane (red, right vertical axis). (c) Profiles of ion (black, left vertical axis) and electron (green, right vertical axis) temperatures measured near the neutral plane. (bottom) Positions of three spacecraft (ThA: black, ThD: red, and ThE: blue) in (x, z) and (x, y) GSM planes.

~100 km/s, just at the B_z peak. The rise of V_x ahead of the front, which has been explained by ion reflection from the DF [see, e.g., *Zhou et al.*, 2010, 2011], is consistent with the acceleration of preexisting plasma by pressure gradients ahead of front and an imbalance between the gradients and the curvature force [*Li et al.*, 2011].

Although the long time intervals of THEMIS observations around $x \sim -12\ R_E$ would allow us to assemble a large database of DF observations, the separation between spacecraft is generally larger than a typical DF's spatial scale; and, thus, current density calculations near DFs often provide smoothed results. Therefore, we restrict our consideration to several examples in which the effect of current reduction can be easily distinguished. Figure 2 shows six THEMIS DF observations. In all, we see a clear reduction of the current density j_y ahead of the DF (demarcated by red arrows). In three of the cases, this reduction is so pronounced that the local j_y becomes negative. Although reversal of j_y is occasionally observed near the neutral plane, cross-tail pressure balance necessitates that the total current $\int_{-L}^{L} j_y dz$ remain positive (L is the plasma sheet thickness). Hence, in the plasma sheet above and below the spacecraft triangle, j_y should be positive. We checked that the lobe magnetic field (equal to the total current $\int_0^L j_y dz$) did not change significantly ahead of DFs. To examine and understand the observed reduction in current density, we next use PIC simulations and compare them with the observations.

3. PIC Simulations

We perform 2-D PIC simulations to explore the potential current density reduction ahead of the DFs and investigate its formation mechanism. The electric and magnetic fields are defined on the grids in the (x, z)

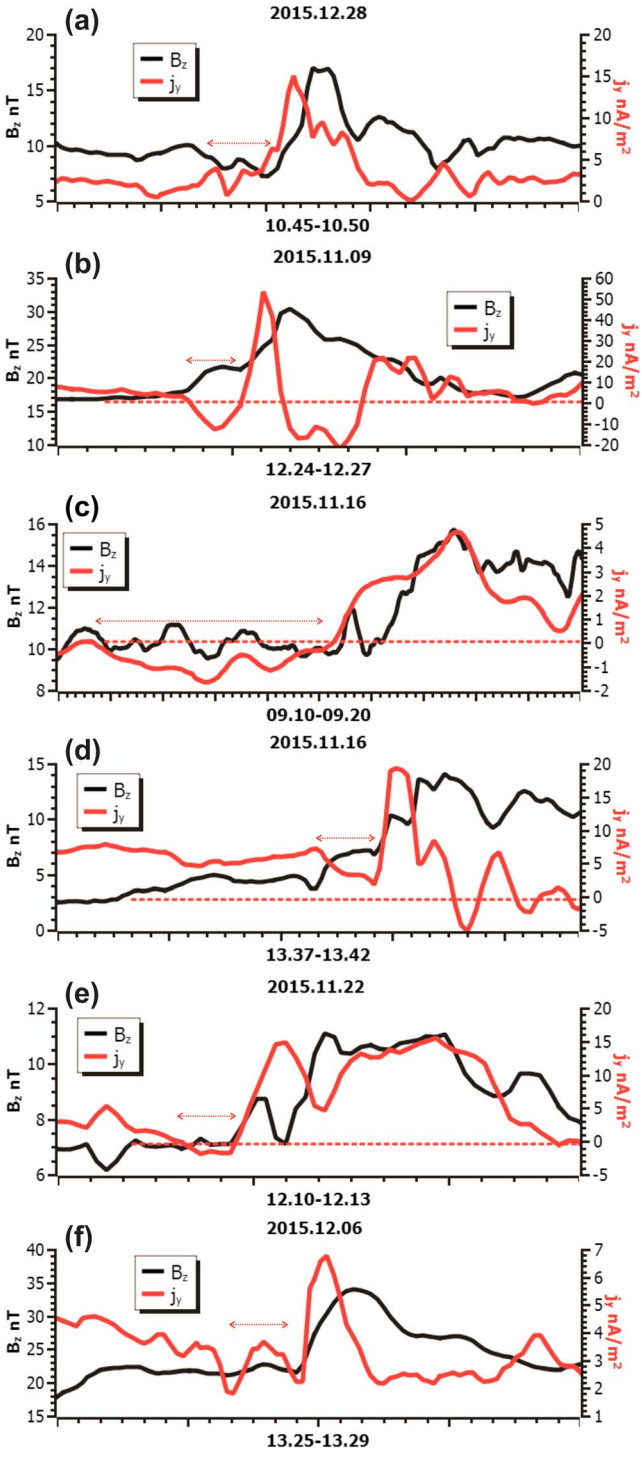

Figure 2. Six DF observations (additional to the one shown in Figure 1) by three THEMIS spacecraft. Each panel shows profiles of B_z measured by the probe near the neutral plane (black, left vertical axis) and current density j_y (red, right vertical axis). Red arrows show the time interval of current density reduction.

plane and updated by solving Maxwell's equations with a full explicit algorithm. The macroparticles, electrons, and ions, are advanced in the electromagnetic fields. The initial equilibrium is a one-dimensional Harris current sheet with an initial magnetic field $\mathbf{B} = B_0 \tanh(z/\delta)\mathbf{e}_x$ and density $n = n_b + n_0 \sec h^2(z/\delta)$, where B_0 is the asymptotic magnetic field, δ is the half width of the current sheet, and n_b is the background plasma density. The initial velocity distributions of the ions and electrons are Maxwellian with drift speed $V_{\alpha 0} = 2T_{\alpha 0}/q_\alpha B_0 \delta$ in the y direction, where $\alpha = i$ and e represent ions and electrons, respectively. We use uniform initial electron and ion temperatures with $T_{i0}/T_{e0} = 5$. Specific parameters for the simulations are $\delta = 0.5d_i$ ($d_i = c/\omega_{pi}$ is the ion inertial length defined by n_0), $n_b = 0.1n_0$, ion-to-electron mass ratio $m_i/m_e = 25$, and light speed $c = 15v_A$, where v_A is the Alfvén speed based on B_0 and n_0. The simulations are performed in a rectangular domain with dimensions $L_x \times L_z = 204.8d_i \times 25.6d_i$, spatial resolution $\Delta x = \Delta z = 0.05d_i$, and temporal resolution $\Delta t = 0.001\ \Omega_i^{-1}$, where $\Omega_i = eB_0/m_i$ is the ion gyrofrequency. In the x direction we use periodic boundary conditions; particles leaving one boundary will enter the simulation domain from the boundary on the opposite side. Conductive boundary conditions are adopted in the z direction; particles are specularly reflected on the conductive boundaries. More than 10^9 particles are employed in the simulations. The simulations are initiated with a small magnetic flux perturbation at the center of the current sheet. The perturbation results in reconnection and development of outflows with enhanced magnetic flux that is consistent with dipolarized flux bundles moving toward Earth.

Figure 3 shows (a) the cross-tail current density, j_y, and the current contributions from (b) electrons, j_{ey}, and (c) ions, j_{iy}, at normalized time $\Omega_i t = 21$. The simulated DF, the interface between the ambient plasma and the recently reconnected dipolarizing flux bundle, is characterized by a sharp B_z increase and is located at

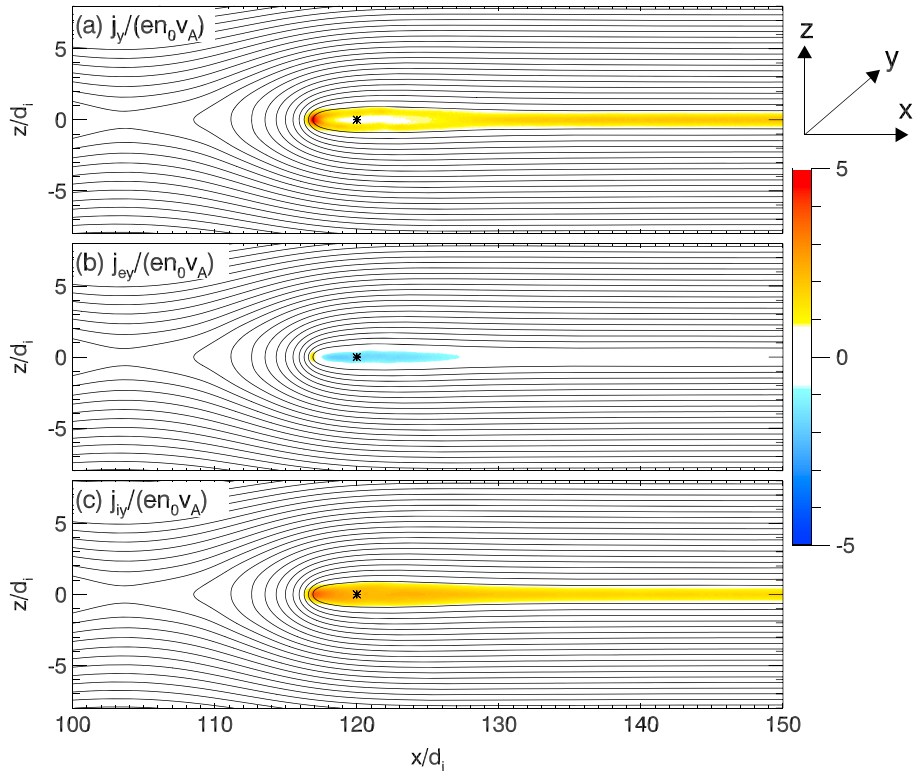

Figure 3. PIC simulation results. The DF propagates along the positive x direction toward the right. (a) Contours of the cross-tail current density $j_y/(\text{env}_A)$, (b) current contribution from electrons, $j_{ey}/(\text{env}_A)$, and (c) current contribution from ions, $j_{iy}/(\text{env}_A)$, at $\Omega_i t = 21$. The solid lines are magnetic field lines, and their spacing indicates magnetic field magnitude.

$x \approx 117d_i$. The DF propagates along the positive x direction toward the right. The cross-tail current density has a peak, $\sim 5en_0v_A$, at the front because of the sharp B_z variation there. The current density at the front is mainly contributed by the ions because of their duskward (positive y) deflection caused by the strong B_z. The cross-tail current density decreases to below en_0v_A from $x \approx 118d_i$ to $127d_i$ ahead of the DF. The current density in the unperturbed current sheet is $2en_0v_A$.

From Figures 3b and 3c, we deduce that the current density reduction ahead of the DF is mainly caused by the dawnward (negative y) current density of the electrons. It is important to note that above and below the neutral plane, the ion current density is increased ahead of the DF (see Figure 3c). This allows the total cross-tail current $\int_{-L}^{L} j_y dz$ to remain almost unchanged, whereas the current density near the neutral plane is reduced significantly. Figure 4 shows the virtual satellite observations at $(x, z) = (120, 0)d_i$ (denoted by an asterisk in Figure 3), which allow us to further investigate the time evolution of the current density reduction ahead of the DF. Note that the DF arrives at $\Omega_i t \approx 21.5$, and B_z reaches its maximum $1.4B_0$ at $\Omega_i t \approx 23$. Ahead of the DF, from $\Omega_i t = 14.5$ to 21.5 (the yellow region in Figure 4), the cross-tail current density j_y begins to decrease from $2en_0v_A$ to $0.5en_0v_A$. The current density reduction ahead of the DF is caused by the increase in electron bulk velocity from $-0.3v_A$ to $1.2v_A$, while the ion bulk velocity remains unchanged (Figure 4c). The plasma (electron and ion) density increases slightly ahead of the DF and then decreases dramatically behind it (a typical DF signature described in *Runov et al.* [2011a, 2015]). The ion temperature increases from $0.5m_iv_A^2$ in the unperturbed current sheet to $0.8m_iv_A^2$ ahead of the DF. Electrons, on the other hand, are mostly heated behind the DF; their relative temperature increase ahead of the DF is less significant than that of the ions.

Given that the current density reduction ahead of the DF is caused by duskward (in the positive y direction) electron flow, which corresponds to dawnward (negative) electron current density, we choose a representative time, $\Omega_i t = 21$ (denoted by the vertical dotted line in Figure 4), when j_y reaches its minimum, to investigate

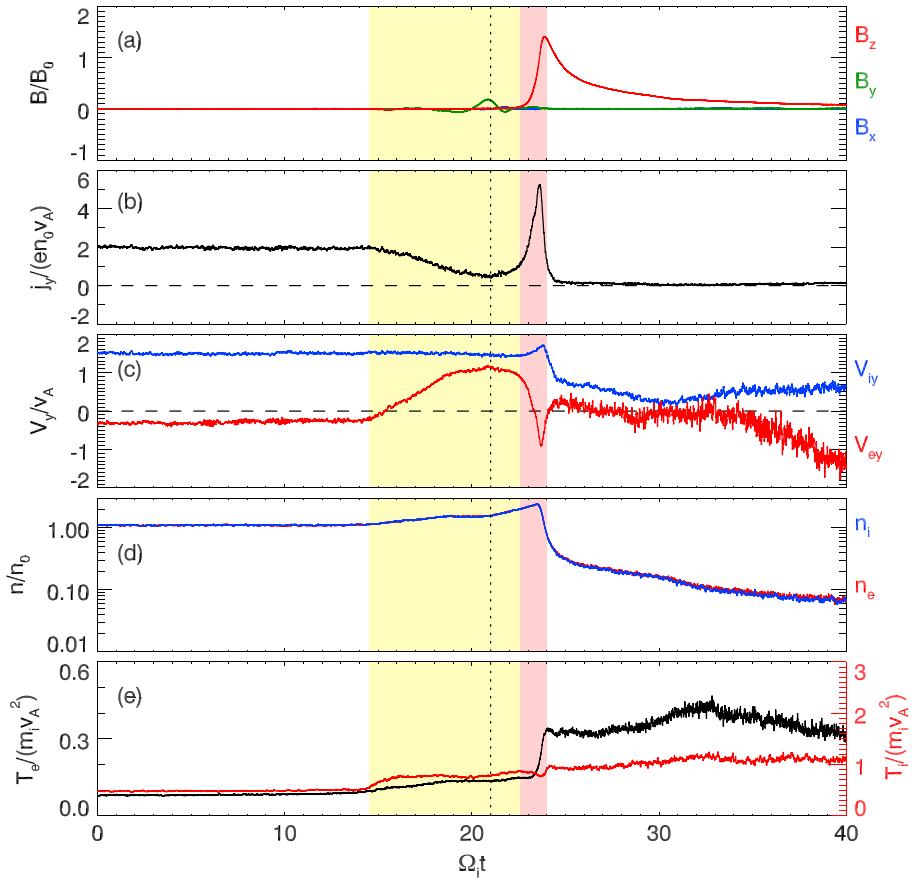

Figure 4. Virtual satellite observations of the (a) magnetic field components B_x/B_0, B_y/B_0, and B_z/B_0; (b) cross-tail current density, $j_y/(\mathrm{env}_A)$; (c) electron and ion bulk velocities in the y direction, V_{ey}/v_A, V_{iy}/v_A; (d) electron and ion densities, n_e/n_0, n_i/n_0; and (e) electron and ion temperatures, $T_e/m_iv_A^2$, $T_i/m_iv_A^2$, versus time at $(x, z) = (120, 0)d_i$ (asterisk in Figure 3).

the formation mechanism of the duskward electron flow. We use the drift approximation to describe the electron bulk velocity [*Northrop*, 1963]

$$\mathbf{V}_e = \mathbf{V}_{\mathrm{E}\times\mathrm{B}} + \mathbf{V}_{e,\mathrm{DM}}, \tag{1}$$

where $\mathbf{V}_{\mathrm{E}\times\mathrm{B}} = \mathbf{E}\times\mathbf{B}/B^2$ is the E-cross-B drift velocity, and $\mathbf{V}_{e,\mathrm{DM}} = -\mathbf{B}\times\nabla p_e/(en_eB^2)$ is the electron diamagnetic drift velocity. For isotropic electrons there is no election curvature drifts induced by thermal anisotropy (i.e., by difference of temperature components along and across the magnetic field). Figure 5a shows E_z, which leads to a duskward (positive y) E-cross-B drift in this region. (Note that the DF propagates in the direction toward the right.) Figures 5b–5d present the y components of $\mathbf{V}_{\mathrm{E}\times\mathrm{B}}$, $\mathbf{V}_{e,\mathrm{DM}}$, and their sum. In the current sheet ahead of the DF, where the cross-tail current density reduces, the large electron duskward flow (or dawnward current) is mostly contributed by the E-cross-B drift. In the unperturbed current sheet (for example, at $x = 140d_i$), however, the electron dawnward flow is much smaller and caused by electron diamagnetic drift. The sum of $\mathbf{V}_{\mathrm{E}\times\mathrm{B}}$ and $\mathbf{V}_{e,\mathrm{DM}}$ shows good consistency with the electron bulk velocity (see Figures 5d and 5e), validating equation (1).

Therefore, the electric field E_z plays an important role in the formation of positive/duskward electron bulk flow, or current density reduction, ahead of the DF. The generation of E_z can be understood from Figure 5f, which plots the charge density. A positive charge density at the center of the current sheet generates the electrostatic field E_z ahead of the DF. The charge originates as follows: ions are reflected and accelerated ahead of the DF [*Zhou et al.*, 2010; *Wu and Shay*, 2012] (electrons are not). This generates a positive j_x (see Figure 5g), although it breaks up because of an instability around $x = 120d_i$ (likely the firehose instability [e.g., *Wu et al.*, 2013] or the Weibel instability [e.g., *Lu et al.*, 2011; *Schoeffler et al.*, 2013]). The above ion reflection/acceleration weakens in the region farther away from the DF, for example,

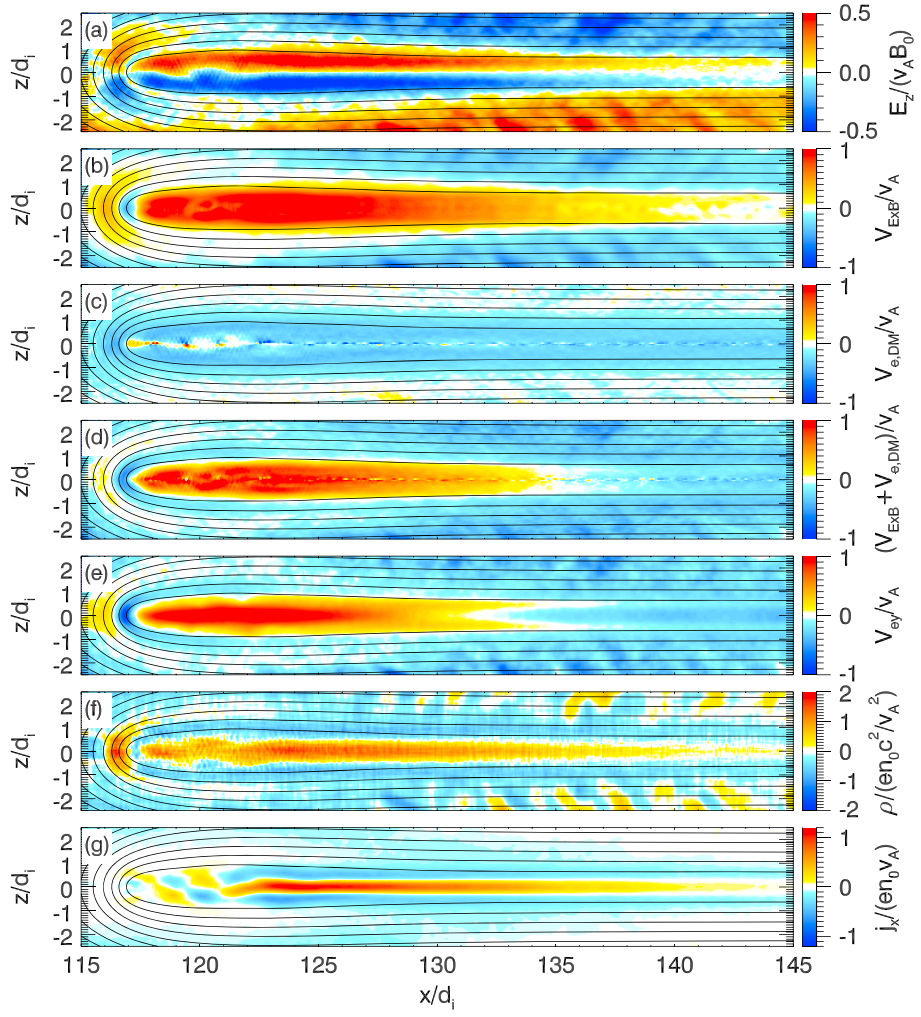

Figure 5. The (a) electric field along the z direction, $E_z/(v_A B_0)$; (b) E-cross-B drift velocity in the y direction, $V_{E\times B}/v_A$; (c) electron diamagnetic drift velocity in the y direction, $V_{e,DM}/v_A$; (d) sum of the electron E-cross-B drift and diamagnetic drift velocities in the y direction, $(V_{E\times B}+V_{e,DM})/v_A$; (e) electron bulk velocity in the y direction, V_{ey}/v_A; (f) charge density, $\rho/\left(en_0c^2/v_A^2\right)$; and (g) current density along the x direction, $j_x/(env_A)$, at $\Omega_i t = 21$. The DF propagates in the direction toward the right. Magnetic field lines (solid lines) are also plotted for reference.

$j_x \approx 1.0en_0v_A$ at $x = 125d_i$ and $j_x \approx 0.3en_0v_A$ at $x = 135d_i$, so $\partial j_x/\partial x > 0$. Therefore, the positive charge density is built up by charge conservation $\partial\rho/\partial t = -\nabla\cdot\mathbf{j} \approx -\partial j_x/\partial x > 0$. This charge density causes the formation of the above E_z directed away from the neutral plane.

4. Summary and Discussion

Using THEMIS observations and PIC simulations, we showed that the current density ahead of DFs is significantly reduced relative to the ambient plasma sheet cross-tail current density. The physical mechanism of this reduction can be summarized as follows:

1. Ions are reflected and accelerated ahead of DFs, and this reflection causes positive charge density buildup.
2. Positive charge density at the equator generates an electrostatic field E_z directed away from the neutral plane ahead of the DFs.
3. Electron positive (duskward) $E_z \times B_x$ drift reduces cross-tail current density. Unlike electrons, ions are demagnetized and do not execute this drift, resulting in a net electron current in the duskward direction that reduces the ambient duskward current.

Previous test particle simulations [*Zhou et al*., 2014b; *Pan et al*., 2015] have suggested that reflected ions can then be deflected dawnward by the (finite) B_z and form a dawnward secondary current. In our PIC simulations, the reflected ion population generates a polarization electric field E_z (i.e., an electrostatic field caused by decoupling of reflected demagnetized ions from magnetized electrons) that drives duskward electron motion (dawnward current) in the absence of a compensating ion current. The previous understanding of current modification in the current sheet ahead of DFs derived in test particle models is modified and improved by our self-consistent model. For a more realistic investigation of this effect, further PIC simulation studies with nonzero B_z initial condition [e.g., *Lembège and Pellat*, 1982; *Schindler and Birn*, 2002; *Sitnov and Schindler*, 2010] are needed.

In the THEMIS observations, current density reduction lasts around 30 s (see red arrows in Figure 2). For a DF propagation speed of about $100-200$ km/s (see Figure 1a and statistics in *Runov et al*., [2011]a), the spatial scale of the current density reduction region is ~4000 km. For a typical ion density of ~0.3 cm^{-3} (see Figure 1b and statistics in *Runov et al*. [2015]), the local ion inertial length d_i is ~300 km. Therefore, the observed spatial scale of current density reduction ahead of DFs is about $13d_i$. In our PIC simulations, the spatial scale of the current density reduction is about $15d_i$ (see Figure 5), which is consistent with the observed value.

In the magnetotail current sheet there is usually a nonzero guide field B_y [e.g., *Petrukovich*, 2011]. Theoretically, a small guide field cannot modify the magnetotail electron kinetics significantly if [e.g., *Hesse et al*., 2004]

$$B_y < (\partial B_x/\partial z)\lambda_{ez}, \tag{2}$$

where λ_{ez} is the electron bounce width in the field reversal given by *Biskamp and Schindler* [1971]:

$$\lambda_{ez} = \left[\frac{2m_eT_e}{e^2(\partial B_x/\partial z)^2}\right]^{1/4}. \tag{3}$$

For $m_e/m_i = 1/25$, $T_e \approx 0.15 m_i v_A^2$, and $\partial B_x/\partial z \approx 0.75 B_0/d_i$ as measured in the simulation for the current density reduction region, equation (2) gives the threshold of the guide field $B_y < 0.29B_0$. We further performed runs with small guide fields, $B_y = 0.1B_0$ and $0.2B_0$, and found that the current density reduction ahead of DFs still exists, showing that the current density reduction is not sensitive to small guide fields in the magnetotail.

We would like to mention that several previous observations have shown that a B_z dip/reduction may be associated with dipolarization front and often occurs just before the leading edge of the front [e.g., *Runov et al*., 2009; *Yao et al*., 2015, and references therein]. In the THEMIS data set shown in Figures 1 and 2, a B_z dip is not observed for all cases. Moreover, Figures 1 and 2 show that a B_z dip can be observed before j_y reduction, or j_y reduction occurs when B_z has already started to dipolarize (increase). Further investigations are needed to identify a possible relation between current density variation responsible for B_z reduction and observed j_y reduction.

Acknowledgments

We acknowledge NASA contract NAS5-02099 for the use of data from the THEMIS Mission. We would like to thank the following people specifically C. W. Carlson and J. P. McFadden for the use of ESA data, D.E. Larson and R.P. Lin for the use of SST data, and K.H. Glassmeier, U. Auster, and W. Baumjohann for the use of FGM data provided under the lead of the Technical University of Braunschweig and with financial support through the German Ministry for Economy and Technology and the German Aerospace Center (DLR) under contract 50 OC 0302. We thank J. Hohl for her assistance in preparation and editing of this paper. We would also like to thank the National Science Foundation of China, grant 41331067, 41527804, 11235009, and 41474125. The THEMIS data were downloaded from http://themis.ssl.berkeley.edu/. The data of simulations can be obtained by contacting the corresponding author through e-mail.

References

Angelopoulos, V., W. Baumjohann, C. F. Kennel, F. V. Coroniti, M. G. Kivelson, R. Pellat, R. J. Walker, H. Luhr, and G. Paschmann (1992), Bursty bulk flows in the inner central plasma sheet, *J. Geophys. Res.*, *97*, 4027–4039, doi:10.1029/91JA02701.

Angelopoulos, V., C. F. Kennel, F. V. Coroniti, R. Pellat, M. G. Kivelson, R. J. Walker, C. T. Russell, W. Baumjohann, W. C. Feldman, and J. T. Gosling (1994), Statistical characteristics of bursty bulk flow events, *J. Geophys. Res.*, *99*, 21,257–21,280, doi:10.1029/94JA01263.

Angelopoulos, V., et al. (2008), First results from the THEMIS mission, *Space Sci. Rev.*, *141*, 453–476, doi:10.1007/s11214-008-9378-4.

Angelopoulos, V., A. Runov, X.-Z. Zhou, D. L. Turner, S. A. Kiehas, S.-S. Li, and I. Shinohara (2013), Electromagnetic energy conversion at reconnection fronts, *Science*, *341*, 1478–1482, doi:10.1126/science.1236992.

Auster, H. U., et al. (2008), The THEMIS fluxgate magnetometer, *Space Sci. Rev.*, *141*, 235–264, doi:10.1007/s11214-008-9365-9.

Biskamp, D., and K. Schindler (1971), Instability of two-dimensional collisionless plasma with neutral points, *Plasma Physics*, *13*, 1013, doi:10.1088/0032-1028/13/11/003.

Deng, X. H., M. Ashour-Abdalla, M. Zhou, R. Walker, M. El-Alaoui, V. Angelopoulos, R. E. Ergun, and D. Schriver (2010), Wave and particle characteristics of earthward electron injections associated with dipolarization fronts, *J. Geophys. Res.*, *115*, A09225, doi:10.1029/2009JA015107.

Dunlop, M. W., A. Balogh, K.-H. Glassmeier, and P. Robert (2002), Four-point Cluster application of magnetic field analysis tools: The curlometer, *J. Geophys. Res.*, *107*, 1384, doi:10.1029/2001JA005088.

Eastwood, J. P., M. V. Goldman, H. Hietala, D. L. Newman, R. Mistry, and G. Lapenta (2015), Ion reflection and acceleration near magnetotail dipolarization fronts associated with magnetic reconnection, *J. Geophys. Res. Space Physics*, *120*, 511–525, doi:10.1002/2014JA020516.

Fu, H. S., Y. V. Khotyaintsev, M. André, and A. Vaivads (2011), Fermi and betatron acceleration of suprathermal electrons behind dipolarization fronts, *Geophys. Res. Lett.*, *38*, L16104, doi:10.1029/2011GL048528.
Fu, H. S., Y. V. Khotyaintsev, A. Vaivads, M. André, and S. Y. Huang (2012a), Electric structure of dipolarization front at sub-proton scale, *Geophys. Res. Lett.*, *39*, L06105, doi:10.1029/2012GL051274.
Fu, H. S., Y. V. Khotyaintsev, A. Vaivads, M. Andre, and S. Y. Huang (2012b), Occurrence rate of earthward-propagating dipolarization fronts, *Geophys. Res. Lett.*, *39*, L10101, doi:10.1029/2012GL051784.
Fu, H. S., Y. V. Khotyaintsev, A. Vaivads, A. Retinò, and M. André (2013), Energetic electron acceleration by unsteady magnetic reconnection, *Nat. Phys.*, *9*, 426–330, doi:10.1038/NPHYS2664.
Gabrielse, C., V. Angelopoulos, A. Runov, and D. L. Turner (2012), The effects of transient, localized electric fields on equatorial electron acceleration and transport toward the inner magnetosphere, *J. Geophys. Res.*, *117*, A10213, doi:10.1029/2012JA017873.
Gabrielse, C., V. Angelopoulos, A. Runov, and D. L. Turner (2014), Statistical characteristics of particle injections throughout the equatorial magnetotail, *J. Geophys. Res. Space Physics*, *119*, 2512–2535, doi:10.1002/2013JA019638.
Ganushkina, N. Y., O. A. Amariutei, Y. Y. Shprits, and M. W. Liemohn (2013), Transport of the plasma sheet electrons to the geostationary distances, *J. Geophys. Res. Space Physics*, *118*, 82–98, doi:10.1029/2012JA017923.
Greco, A., A. Artemyev, and G. Zimbardo (2014), Proton acceleration at two-dimensional dipolarization fronts in the magnetotail, *J. Geophys. Res. Space Physics*, *119*, 8929–8941, doi:10.1002/2014JA020421.
Hesse, M., M. Kuznetsova, and J. Birn (2004), The role of electron heat flux in guide-field magnetic reconnection, *Phys. Plasmas*, *11*, 5387–5397 , doi:10.1063/1.1795991.
Huang, S. Y., M. Zhou, X. H. Deng, Z. G. Yuan, Y. Pang, Q. Wei, W. Su, H. M. Li, and Q. Q. Wang (2012), Kinetic structure and wave properties associated with sharp dipolarization front observed by Cluster, *Ann. Geophys.*, *30*, 97–107, doi:10.5194/angeo-30-97-2012.
Lembège, B., and R. Pellat (1982), Stability of a thick two-dimensional quasineutral sheet, *Phys. Fluids*, *25*, 1995, doi:10.1063/1.863677.
Li, J.-Z., X.-Z. Zhou, V. Angelopoulos, J. Liu, A. Runov, D.-X. Pan, and Q.-G. Zong (2016), Contribution of ion reflection to the energy budgets of dipolarization fronts, *Geophys. Res. Lett.*, *43*, 493–500, doi:10.1002/2015GL067300.
Li, S.-S., V. Angelopoulos, A. Runov, X.-Z. Zhou, J. McFadden, D. Larson, J. Bonnell, and U. Auster (2011), On the force balance around dipolarization fronts within bursty bulk flows, *J. Geophys. Res.*, *116*, A00I35, doi:10.1029/2010JA015884.
Lin, Y., X. Y. Wang, S. Lu, J. D. Perez, and Q. M. Lu (2014), Investigation of storm-time magnetotail and ion injection using three-dimensional global hybrid simulation, *J. Geophys. Res. Space Physics*, *119*, 7413–7432, doi:10.1002/2014JA020005.
Liu, J., C. Gabrielse, V. Angelopoulos, N. A. Frissell, L. R. Lyons, J. P. McFadden, J. Bonnell, and K. H. Glassmeier (2011), Superposed epoch analysis of magnetotail flux transport during substorms observed by THEMIS, *J. Geophys. Res.*, *116*, A00129, doi:10.1029/2010JA015886.
Liu, J., V. Angelopoulos, A. Runov, and X.-Z. Zhou (2013a), On the current sheets surrounding dipolarizing flux bundles in the magnetotail: The case for wedgelets, *J. Geophys. Res. Space Physics*, *118*, 2000–2020, doi:10.1002/jgra.50092.
Liu, J., V. Angelopoulos, X.-Z. Zhou, A. Runov, and Z. H. Yao (2013b), On the role of pressure and flow perturbations around dipolarizing flux bundles, *J. Geophys. Res. Space Physics*, *118*, 7104–7118, doi:10.1002/2013JA019256.
Liu, J., V. Angelopoulos, X.-Z. Zhou, and A. Runov (2014), Magnetic flux transport by dipolarizing flux bundles, *J. Geophys. Res. Space Physics*, *119*, 909–926, doi:10.1002/2013JA019395.
Liu, J., V. Angelopoulos, X. Chu, X.-Z. Zhou, and C. Yue (2015), Substorm current wedge composition by wedgelets, *Geophys. Res. Lett.*, *42*, 1669–1676, doi:10.1002/2015GL063289.
Lu, S., Q. M. Lu, X. Shao, P. H. Yoon, and S. Wang (2011), Weibel instability and structures of magnetic island in anti-parallel collisionless magnetic reconnection, *Phys. Plasmas*, *18*, 072105, doi:10.1063/1.3605029.
Lu, S., et al. (2015), Dipolarization fronts as earthward propagating flux ropes: A three-dimensional global hybrid simulation, *J. Geophys. Res. Space Physics*, *120*, 6286–6300, doi:10.1002/2015JA021213.
McFadden, J. P., C. W. Carlson, D. Larson, M. Ludlam, R. Abiad, B. Elliot, P. Turin, M. Marckwordt, and V. Angelpoulos (2008), The THEMIS ESA plasma instrument and in-flight calibration, *Space Sci. Rev.*, *141*, 277–302, doi:10.1007/s11214-008-9440-2.
McPherron, R. L., C. T. Russell, and M. P. Aubry (1973), Satellite studies of magnetospheric substorms on August 15, 1968: 9. Phenomenological model for substorms, *J. Geophys. Res.*, *78*, 3131–3149, doi:10.1029/JA078i016p03131.
Moore, T., R. Arnoldy, J. Feynman, and D. Hardy (1981), Propagating substorm injection fronts, *J. Geophys. Res.*, *86*, 6713–6726, doi:10.1029/JA086iA08p06713.
Nakamura, R., et al. (2002), Motion of the dipolarization front during a flow burst event observed by Cluster, *Geophys. Res. Lett.*, *29*, 1942, doi:10.1029/2002GL015763.
Nakamura, R., et al. (2011), Flux transport, dipolarization, and current sheet evolution during a double-onset substorm, *J. Geophys. Res.*, *116*, A00I36, doi:10.1029/2010JA015865.
Northrop, T. G. (1963), *The Adiabatic Motion of Charged Particles*, Interscience Publishers John Wiley, New York-London-Sydney.
Pan, D.-X., X.-Z. Zhou, Q.-Q. Shi, J. Liu, V. Angelopoulos, A. Runov, Q.-G. Zong, and S.-Y. Fu (2015), On the generation of magnetic dips ahead of advancing dipolarization fronts, *Geophys. Res. Lett.*, *42*, 4256–4262, doi:10.1002/2015GL064369.
Panov, E. V., A. V. Artemyev, W. Baumjohann, R. Nakamura, and V. Angelopoulos (2013), Transient electron precipitation during oscillatory BBF braking: THEMIS observations and theoretical estimates, *J. Geophys. Res. Space Physics*, *118*, 3065–3076, doi:10.1002/jgra.50203.
Petrukovich, A. A. (2011), Origins of plasma sheet By, *J. Geophys. Res.*, *116*, A07217, doi:10.1029/2010JA016386.
Runov, A., V. Angelopoulos, M. I. Sitnov, V. A. Sergeev, J. Bonnell, J. P. McFadden, D. Larson, K. H. Glassmeier, and U. Auster (2009), THEMIS observations of an earthward-propagating dipolarization front, *Geophys. Res. Lett.*, *36*, L14106, doi:10.1029/2009GL038980.
Runov, A., V. Angelopoulos, X. Z. Zhou, X. J. Zhang, S. Li, F. Plaschke, and J. Bonnell (2011a), A THEMIS multicase study of dipolarization fronts in the magnetotail plasma sheet, *J. Geophys. Res.*, *116*, A05216, doi:10.1029/2010JA016316.
Runov, A., et al. (2011b), Dipolarization fronts in the magnetotail plasma sheet, *Planet. Space Sci.*, *59*, 517–525, doi:10.1016/j.pss.2010.06.006.
Runov, A., V. Angelopoulos, C. Gabrielse, J. Liu, D. L. Turner, and X.-Z. Zhou (2015), Average thermodynamic and spectral properties of plasma in and around dipolarizing flux bundles, *J. Geophys. Res. Space Physics*, *120*, 4369–4383, doi:10.1002/2015JA021166.
Russell, C. T., and R. L. McPherron (1973), The magnetotail and substorms, *Space Sci. Rev.*, *15*, 205–266, doi:10.1007/BF00169321.
Schindler, K., and J. Birn (2002), Models of two-dimensional embedded thin current sheets from Vlasov theory, *J. Geophys. Res.*, *107*, A81193, doi:10.1029/2001JA000304.
Schmid, D., M. Volwerk, R. Nakamura, W. Baumjohann, and M. Heyn (2011), A statistical and event study of magnetotail dipolarization fronts, *Ann. Geophys.*, *29*, 1537–1547, doi:10.5194/angeo-29-1537-2011.
Schmid, D., R. Nakamura, F. Plaschke, M. Volwerk, and W. Baumjohann (2015), Two states of magnetotail dipolarization fronts: A statistical study, *J. Geophys. Res. Space Physics*, *120*, 1096–1108, doi:10.1002/2014JA020380.

Schoeffler, K. M., J. F. Drake, M. Swisdak, and K. Knizhnik (2013), The role of pressure anisotropy on particle acceleration during magnetic reconnection, *Astrophys. J.*, *764*, 126, doi:10.1088/0004-637X/764/2/126.

Sergeev, V., V. Angelopoulos, S. Apatenkov, J. Bonnell, R. Ergun, R. Nakamura, J. McFadden, D. Larson, and A. Runov (2009), Kinetic structure of the sharp injection/dipolarization front in the flow-braking region, *Geophys. Res. Lett.*, *36*, L21105, doi:10.1029/2009GL040658.

Sitnov, M. I., and K. Schindler (2010), Tearing stability of a multiscale magnetotail current sheet, *Geophys. Res. Lett.*, *37*, L08102, doi:10.1029/2010GL042961.

Sitnov, M. I., M. Swisdak, and A. V. Divin (2009), Dipolarization fronts as a signature of transient reconnection in the magnetotail, *J. Geophys. Res.*, *114*, A04202, doi:10.1029/2008JA013980.

Sun, W. J., S. Y. Fu, G. K. Parks, J. Liu, Z. H. Yao, Q. Q. Shi, Q.-. G. Zong, S. Y. Huang, Z. Y. Pu, and T. Xiao (2013), Field-aligned currents associated with dipolarization fronts, *Geophys. Res. Lett.*, *40*, 4503–4508, doi:10.1002/grl.50902.

Ukhorskiy, A. Y., M. I. Sitnov, V. G. Merkin, and A. V. Artemyev (2013), Rapid acceleration of protons upstream of earthward propagating dipolarization fronts, *J. Geophys. Res. Space Physics*, *118*, 4952–4962, doi:10.1002/jgra.50452.

Wu, M. Y., M. Volwerk, Q. M. Lu, Z. Vörös, R. Nakamura, and T. L. Zhang (2013), The proton temperature anisotropy associated with bursty bulk flows in the magnetotail, *J. Geophys. Res. Space Physics*, *118*, 4875–4883, doi:10.1002/jgra.50451.

Wu, P., and M. A. Shay (2012), Magnetic dipolarization front and associated ion reflection: Particle-in-cell simulations, *Geophys. Res. Lett.*, *39*, L08107, doi:10.1029/2012GL051486.

Yang, J., F. R. Toffoletto, R. A. Wolf, S. Sazykin, P. A. Ontiveros, and J. M. Weygand (2012), Large-scale current systems and ground magnetic disturbance during deep substorm injections, *J. Geophys. Res.*, *117*, A04223, doi:10.1029/2011JA017415.

Yao, Z. H., et al. (2013), Current structures associated with dipolarization fronts, *J. Geophys. Res. Space Physics*, *118*, 6980–6985, doi:10.1002/2013JA019290.

Yao, Z. H., et al. (2015), A physical explanation for the magnetic decrease ahead of dipolarization fronts, *Ann. Geophys.*, *33*, 1301–1309, doi:10.5194/angeo-33-1301-2015.

Zhou, X.-Z., V. Angelopoulos, J. Liu, A. Runov, and D.-X. Pan (2014a), Asymmetric braking and dawnward deflection of dipolarization fronts: Effects of ion reflection, *Geophys. Res. Lett.*, *41*, 6994–7001, doi:10.1002/2014GL061794.

Zhou, X.-Z., V. Angelopoulos, J. Liu, A. Runov, and S.-S. Li (2014b), On the origin of pressure and magnetic perturbations ahead of dipolarization fronts, *J. Geophys. Res. Space Physics*, *119*, 211–220, doi:10.1002/2013JA019394.

Zhou, X.-. Z., V. Angelopoulos, V. A. Sergeev, and A. Runov (2010), Accelerated ions ahead of earthward propagating dipolarization fronts, *J. Geophys. Res.*, *115*, A00I03, doi:10.1029/2010JA015481.

Zhou, X.-. Z., V. Angelopoulos, V. A. Sergeev, and A. Runov (2011), On the nature of precursor flows upstream of advancing dipolarization fronts, *J. Geophys. Res.*, *116*, A03222, doi:10.1029/2010JA016165.